We are IntechOpen, the world's leading publisher of Open Access books Built by scientists, for scientists

6,900
Open access books available

186,000
International authors and editors

200M
Downloads

Our authors are among the

154
Countries delivered to

TOP 1%
most cited scientists

12.2%
Contributors from top 500 universities

CLARIVATE ANALYTICS
BOOK CITATION INDEX
INDEXED

WEB OF SCIENCE™

Selection of our books indexed in the Book Citation Index
in Web of Science™ Core Collection (BKCI)

Interested in publishing with us?
Contact book.department@intechopen.com

Transient Modelling of Ultra Wideband (UWB) Pulse Propagation

Qingsheng Zeng and Arto Chubukjian
Communications Research Centre Canada
Ottawa, Ontario K2H 8S2, Canada

1. Introduction

Transient modeling of electromagnetic pulse propagation can be traced back to the beginning of the last century, has become a powerful tool for ultra wideband (UWB) technology, and has been of great interest with a variety of applications, such as short range communication, material characterization, geophysical probing and medical imaging. When an appropriate model has been adopted for the medium, one can manage to work out the frequency-domain solution for wave propagation in this medium. The main difficulties are encountered when trying to transform from the frequency-domain to the time-domain. An inverse fast Fourier transform (IFFT) can be employed to yield the desired transient result. However, several investigations have shown that a large number of sample points are required if one desires to reduce aliasing so that an accurate characterization can be obtained. Besides, when a frequency-domain solution has singular behaviors at some frequencies, direct use of IFFT is inappropriate and some preprocessing must be done for removing these singularities. Furthermore, it is preferable to solve the problems directly in the time-domain under certain circumstances, in which time-varying media or nonlinear systems are involved, or a time-domain response persists very long time.

Other techniques have their own inherent problems. Numerical integration algorithms are free from the problem of aliasing, but the highly oscillatory integrands that are encountered mandate a large number of sample points for the integration and correspondingly a relatively large amount of computation time. Asymptotic techniques are computationally efficient and provide valuable insight into the physical mechanism. However, an asymptotic analysis can be quite cumbersome and the resulting asymptotic expressions can be applied only to parameter values that fall within the range of applicability for the asymptotic expansion. The finite-difference time-domain (FDTD) technique has the advantage that it can be applied to relatively complex, inhomogeneous media, but it also has the following disadvantages. Firstly, the FDTD method does not accurately fulfill the boundary conditions at material interfaces posed by Maxwell's equations, and can cause high calculation costs even in combination with surface impedance boundary conditions for achieving high accuracy under some circumstances. Secondly, when the widths of signal pulses are very narrow and the calculation time domain is large, FDTD solutions may become

computationally intractable. Thirdly, the standard FDTD approach cannot handle simulations of long propagation distances because of finite computer memory resources and accumulation of phase errors associated with numerical dispersion. Another common drawback of the FDTD technique, fast Fourier transform (FFT) and numerical integration is that all the three techniques are purely numerical, and therefore it is difficult to extract the physical phenomenology from the numerical data.

The advancement of UWB technology has been driving the need to develop efficient techniques for transient analyses of electromagnetic pulses. The objective of this chapter is to introduce some new technique that is based on numerical inversion of Laplace transform into transient modeling of UWB pulse propagation. In this chapter, first of all, the previous related investigations, majority of which are not based either on FFT, or on FDTD, or on other purely numerical methods, are overviewed, and some limitations of these methods are discussed. Then numerical inversion of Laplace transform and Prony's method are addressed. Next, the approach combining a numerical inversion of the Laplace transform with Prony's method is applied to the analyses of pulses reflected from a conductive interface. Meanwhile, a mathematical proof is presented, showing that the numerical inversion of the Laplace transform is applicable to the characterization of the reflected pulse due to an incident pulse that is a linear combination of exponential signals and is impinging upon a conductive interface at any incident angle for both horizontal and vertical polarizations. Numerical results are illustrated and compared with those published in the literature. A good agreement between the two validates the correctness and effectiveness of this approach. Furthermore, a time domain multipath model is utilized to characterize hallway UWB signal propagation. With the evaluation of direct and reflected waves in time domain, the performance analysis is conducted for binary UWB communications, and the impacts of multipath components on pulse distortion and UWB system performance are discussed. After that, based on the studies of pulses reflected from a conducting half space, characterization of pulses propagating through a lossy dielectric slab is pursued. Our results are shown to be comparable to the previously published results and agree well with those obtained using the FDTD technique. Moreover, the transmission loss is discussed for different parameters and the results are shown to be consistent with those published in the literature. The corresponding results for an incident angle close to 90^0 are also provided, which can not be generated with the previous approaches. In addition, the concern on whether the treatment of permittivity and conductivity in this chapter accords with the Kramers–Kronig relations is properly adressed. Finally, this approach is summarized and the significance of this work is discussed.

2. Overview of Previous Investigations

Theoretical investigations of pulse propagation through different media and interaction with objects have been performed since the days of Sommerfeld during the early last century (Sommerfeld, 1914). These investigations involved calculations of the reflected and/or transmitted fields at the interface between two different media. The problem involving a time-harmonic plane wave obliquely incident on a finite conductive half-space is a classic boundary value problem in electromagnetic theory that is thoroughly treated in standard textbooks, for instance, those by Stratton (Stratton, 1941) and by Balanis (Balanis,

1989). However, due to the mathematical complexity, it is not easy to analytically integrate the required inverse Laplace transform. Dudley et al. (Dudley et al., 1974) undertook a thorough investigation of TE and TM reflected waves associated with a double exponential, obliquely incident plane wave. They utilized contour integration techniques to rewrite the inverse Fourier transform representation for the reflected fields in terms of a residue term and an integral around the branch cut. The contribution of this branch cut was calculated using numerical integration. Papazoglou (Papazoglou, 1975) extended the analysis to the treatment of TE and TM transmitted waves. He also studied a Debye model which accounted for the frequency dependence in the electrical properties of the conductive media. Klaasen (Klaasen, 1990) showed that the TE transmitted and reflected fields associated with a unit-step, obliquely incident plane wave can be represented in terms of convolution integrals involving exponential functions and modified Bessel functions. Klassen employed a time marching procedure to evaluate the required convolution integrals. The FDTD technique was applied to this problem (Maloney et al., 1990), but computation costs are high even in combination with surface impedance boundary conditions (Maloney & Smith, 1992). The approximate form of a frequency-domain reflection coefficient permits one analytical expression for the impulse response of a lossy half space (Barnes & Tesche, 1991), but makes the solutions inaccurate or even invalid in some cases, e.g., for large incident angles relative to the normal to the interface and/or for relative dielectric constants below the order of 10. Pao et al (Pao et al, 1996, a) (Pao et al, 1996, b) developed a method for the analytical evaluation of the inverse Laplace transform representations for transient TE and TM plane waves, obliquely incident on a conductive half space. They assumed that the permittivity and conductivity of the dispersive half space are independent of frequency. The time-domain expressions for the reflected and transmitted waves are first represented as inverse Laplace transform. The transient fields are then shown to consist of two canonical integrals that in turn are solved analytically, thus leading to solutions involving incomplete Lipschitz-Hankel integrals (ILHI's). Rothwell and Suk introduced a rapidly converging series of the time-domain reflection coefficient into the analysis of transient reflection from a lossy half space, which is valid for all incident angles for the horizontal polarization (Rothwell & Suk, 2003), and for incident angles less than the Brewster angle for the vertical polarization (Rothwell, 2005). Few terms provide good accuracy for late time, while many more terms may be required to approach acceptable accuracy for early time. Pantoja et al (Pantoja et al., 2009) compared the method in (Rothwell & Suk, 2003) (Rothwell, 2005) with that in (Barnes & Tesche, 1991) by changing angles of incidence and constitutive parameters of half-spaces, and presented the accuracy and errors for the direct computation of the time-domain plane wave reflection coefficients for TE and TM plane waves incident on a lossy half-space.

3. Numerical Inversion of Laplace Transform and Prony's Method

3.1 Numerical Inversion of Laplace Transform

The Laplace transform (image function in the complex frequency domain) $F(s)$ and the inverse Laplace transform (original function in the time domain) $f(t)$ are related by the forward transformation

$$Lf(t) = F(s) = \int_0^\infty f(t)e^{-st}dt \tag{1}$$

and the inverse transformation

$$L^{-1}F(s) = f(t) = \frac{1}{2\pi j}\int_{\gamma-j\infty}^{\gamma+j\infty} F(s)e^{st}ds .$$
(2)

In general, it is straightforward to take the Laplace transform of a function. However, the inverse transformation is often difficult. In many cases, the method using simple rules and a table of transforms, and the method using the Bromwich integral and Cauchy integral theorem do not work well, and some numerical technique must be utilized. In this work, the method proposed by Hosono (Hosono, 1981) is applied. To implement the numerical inversion method, the following conditions should be satisfied: 1) $F(s)$ is defined for $\text{Re}(s) > 0$; 2) $F(s)$ is nonsingular; 3) $\lim_{s\to\infty} F(s) = 0$ for $\text{Re}(s) > 0$; 4) $F^*(s) = F(s^*)$, where the asterisk denotes complex conjugate.

The most distinctive feature of this method lies in the approximation for e^{st}. Its main points are:

i)
$$e^{st} = \lim_{\rho\to\infty} \frac{e^{\rho}}{2\cosh(\rho-st)} = e^{st} - e^{-2\rho}e^{3st} + e^{-4\rho}e^{5st} - \cdots$$
(3)

ii)
$$e^{st} \approx E_{ec}(st,\rho) = \frac{e^{\rho}}{2\cosh(\rho-st)} = \frac{e^{\rho}}{2}\sum_{n=-\infty}^{\infty} \frac{(-1)^n j}{st - [\rho + j(n-0.5)\pi]}$$
(4)

iii) The Bromwich integral is transformed to the integral around the poles of $E_{ec}(st,\rho)$.

Then $f(t)$ is approximated by $f_{ec}(t,\rho)$, which is expressed by

$$f_{ec}(t,\rho) = \frac{1}{2\pi j}\int_{\gamma-j\infty}^{\gamma+j\infty} F(s)E_{ec}(st,\rho)\,ds = f(t) - e^{-2\rho}f(3t) + e^{-4\rho}f(5t) - \cdots = (e^{\rho}/t)\sum_{n=1}^{\infty} F_n$$
(5)

where $t > 0$, and

$$F_n = (-1)^n \text{Im} F\{[\rho + j(n-0.5)\pi]/t\}$$
(6)

Equation (5) shows that the function $f_{ec}(t,\rho)$ gives a good approximation to $f(t)$ when $\rho \gg 1$, and can be used for error estimation. Equations (5) and (6) are derived by substituting $E_{ec}(st,\rho)$ from (4), and can be applied to the numerical inversion of the Laplace transform. In practice, the infinite series in (5) has to be truncated after a proper number of terms. Since the infinite series is a slowly convergent alternating series, truncating to a small number of terms leads to a significant error. An effective approach using the Euler transformation has been developed, which works under the following conditions (Hosono, 1981): a) There exists an integer $k \geq 1$ such that the signs of F_n alternate for $n \geq k$; b) For $n \geq k$, $\frac{1}{2} < |F_{n+1}/F_n| \leq 1$. With conditions a) and b), (5) can be truncated with $f_{ec}^{lm}(t,a)$, which has $N = l + m$ terms and is given by

$$f_{ec}^{lm}(t,\rho) = \left(e^{\rho}/t\right)\left(\sum_{n=1}^{l-1} F_n + 2^{-m-1}\sum_{n=0}^{m} A_{mn}F_{l+n}\right) \tag{7}$$

where A_{mn} are defined recursively by

$$A_{mm} = 1, \qquad\qquad A_{mn-1} = A_{mn} + \binom{m+1}{n}. \tag{8}$$

In this method, the upper bound for the truncation errors is given by

$$R^{lm} = \left|f_{ec}^{l+1,m}(t,\rho) - f_{ec}^{l,m}(t,\rho)\right| \tag{9}$$

while the upper bound for the approximation errors is given by

$$\left|f_{ec}(t,\rho) - f(t)\right| \approx M e^{-2\rho}, \tag{10}$$

If

$$\left|f(t)\right| \leq M \qquad \text{for all} \quad t > 0.$$

As indicated in (10), the relative approximation errors are less than $e^{-2\rho}$, while the truncation errors increase with t and decrease with N. For a typical value of t, the calculation is repeated by increasing N to determine a proper number of terms in (5), which makes the truncation errors small enough.

3.2 Prony's Method and Its Application to Decomposition of UWB Signals

An incident signal can be represented as a superposition of exponential functions, i.e.,

$$E(t) = \sum_{p=1}^{q} C_p e^{-\alpha_p t} \tag{11}$$

where q is the number of exponential functions, and can be infinite or a finite number. In this article, only the case where q is finite or can be truncated to a finite is considered. C_p and α_p can be determined directly from one set of sample values of $E(t)$. This technique is known as Prony's method. When α_p is nonnegative, C_p is a real; when α_p is a complex number with a nonnegative real part, C_p is a complex number, and the corresponding conjugate term, $C_p^* e^{-\alpha^* t}$, must be included in (11) in this case.

Following the discussion of Prony's method in (Zeng, 2010), q is selected through a series of numerical trials to meet some requirement of accuracy. In this work, a Gaussian doublet is used as the incident pulse. For approximating a Gaussian doublet by a series of exponentials within some time interval, the numerical trials in (Zeng, 2010) show that the accumulative error first decreases rapidly with the number of exponentials, and then does

not significantly decrease if the number of exponentials is above 20. Hence, more than 20 exponential functions should be used for approximating a Gaussian doublet pulse with good accuracy.

4. Reflection of UWB Pulses from a Conducting Half Space

In this section, how to apply the above approach to modeling pulses reflected from a conductive interface is demonstrated, and the comparisons between our results and the published ones are made, showing a good agreement between them. A pulse which is a linear combination of a finite number of exponential functions is expressed by (11), and is incident from free space onto an interface between free space and a lossy material with conductivity σ and relative dielectric constant ε_r. The reflection coefficients in complex frequency domain for vertical and horizontal polarizations are

$$R_v(s) = \frac{\left(\varepsilon_r + \dfrac{\sigma}{s\varepsilon_0}\right)cos\,\theta - \sqrt{\varepsilon_r + \dfrac{\sigma}{s\varepsilon_0} - sin^2\theta}}{\left(\varepsilon_r + \dfrac{\sigma}{s\varepsilon_0}\right)cos\,\theta + \sqrt{\varepsilon_r + \dfrac{\sigma}{s\varepsilon_0} - sin^2\theta}} \tag{12}$$

and

$$R_h(s) = \frac{cos\,\theta - \sqrt{\varepsilon_r + \dfrac{\sigma}{s\varepsilon_0} - sin^2\theta}}{cos\,\theta + \sqrt{\varepsilon_r + \dfrac{\sigma}{s\varepsilon_0} - sin^2\theta}}\,, \tag{13}$$

respectively, where ε_0 is the permittivity of free space, θ is the incidence angle relative to the normal to the interface, and s is the complex frequency. The image function of $E(t)$ in (11) is

$$E(s) = \sum_{p=1}^{q} \frac{C_p}{s + \alpha_p} \tag{14}$$

The final image functions, $F_v(s) = R_v(s)E(s)$ and $F_h(s) = R_h(s)E(s)$, obviously satisfy conditions 1) – 4) listed in Section 3. A proof is given below that, for $s = \left[\rho + j(n - 0.5)\pi\right]/t$, $F_v(s)$ and $F_h(s)$ also obey the above two conditions a) and b) described in Section 3, under which $f_{ec}^{lm}(t,\rho)$ can be used to approximate $f_{ec}(t,\rho)$.

Here only the proof for $F_v(s)$ with α_p and C_p being real numbers is given, since the proofs for $F_v(s)$ with α_p and C_p being complex numbers and for $F_h(s)$ are similar. If we let

$$\left(\varepsilon_r + \frac{\sigma}{s\varepsilon_0}\right)cos\,\theta = a + jb\,, \tag{15}$$

$$\varepsilon_r + \frac{\sigma}{s\varepsilon_0} - sin^2\theta = c_1 + jd_1 , \tag{16}$$

$$\sqrt{\varepsilon_r + \frac{\sigma}{s\varepsilon_0} - sin^2\theta} = c + jd , \tag{17}$$

$$a = \left(\varepsilon_r + \frac{\rho\sigma t}{B}\right)cos\theta , \quad b = -\frac{(n-0.5)\pi\sigma t}{B}cos\theta , \quad B = \left[\rho^2 + (n-0.5)^2\pi^2\right]\varepsilon_0 , \tag{18}$$

$$c_1 = \varepsilon_r - sin^2\theta + \frac{\rho\sigma t}{B} , \qquad d_1 = -\frac{(n-0.5)\pi\sigma t}{B} , \tag{19}$$

$$c = \pm\sqrt{\frac{c_1 + \sqrt{c_1^2 + d_1^2}}{2}} , \qquad d = \pm\frac{d_1}{|d_1|}\sqrt{\frac{\sqrt{c_1^2 + d_1^2} - c_1}{2}} . \tag{20}$$

If we denote

$$\sum_{p=1}^{q} \frac{C_p}{s + \alpha_p} = \sum_{p=1}^{q}\left(u_p + jv_p\right) , \tag{21}$$

then

$$u_p = \frac{(\rho + \alpha_p t)C_p t}{A} , \quad v_p = -\frac{(n-0.5)\pi C_p t}{A} , \quad A = (\rho + \alpha_p t)^2 + (n-0.5)^2\pi^2 . \tag{22}$$

From $F_v(s) = R_v(s)E(s)$,

$$F_v(s) = \sum_{p=1}^{q} \frac{(a+jb)-(c+jd)}{(a+jb)+(c+jd)}\left(u_p + jv_p\right) , \tag{23}$$

then

$$F_n = (-1)^n Im\left(F_v(s)\right) = (-1)^n\frac{F_v(s) - F_v^*(s)}{2j} = \sum_{p=1}^{q}\frac{(-1)^n\left(v_p g + u_p h\right)}{(a+c)^2 + (b+d)^2} , \tag{24}$$

where

$$g = (a^2 + b^2) - (c^2 + d^2) , \qquad h = 2(bc - ad) . \tag{25}$$

When n becomes large,

$$F_n \rightarrow \sum_{p=1}^{q}(-1)^n\left(-\frac{C_p t}{n\pi}\right)\frac{\varepsilon_r cos\theta - \sqrt{\varepsilon_r - sin^2\theta}}{\varepsilon_r cos\theta + \sqrt{\varepsilon_r - sin^2\theta}} .$$

Thus, the signs of F_n alternate, and furthermore, $|F_{n+1}| < |F_n|$ but $|F_{n+1}| \rightarrow |F_n|$, viz., $F_v(s)$ satisfies the two conditions a) and b) described in Section 3.

For comparing our result with that in (Qiu, 2004), the same Gaussian doublet pulse as that in (Qiu, 2004) is used as the incident pulse, which is the second derivative of a Gaussian pulse and is given by

$$E(t) = \left[1 - 4\pi\left(\frac{t - t_s}{\tau_p}\right)^2\right]\exp\left(-2\pi\left(\frac{t - t_s}{\tau_p}\right)^2\right) \qquad (26)$$

where the amplitude has been normalized to unity, the waveform parameter $\tau_p = 1.7262$ ns and the time shift $t_s = 0.75$ ns in the calculation. Fig. 1 plots the incident pulse and the approximating pulse with 40 exponential functions, showing a good approximation.

Equations (12) and (13) are used for the final image functions. The reflected field is calculated when $\theta = 45^0$, $\varepsilon_r = 10, 25, 40$ and $\sigma = 0.1$ mho/m, and is plotted in Fig. 2 and in Fig. 3 for the horizontal and vertical polarizations, respectively. These two figures illustrate that the reflected pulse has less distortion for both polarizations in this case, and the peak amplitude of the reflected pulse increases with the increase of ε_r. Comparison between the two figures indicates that the reflected pulse has smaller peak amplitudes for the vertical polarization than for the horizontal polarization. Fig. 3 compares our results with those in (Qiu, 2004) and shows a good agreement between them. It is worthwhile to point out that the result in (Qiu, 2004) is accurate in this case where the incident angle is not large and the relative electric constant is on the order of 10.
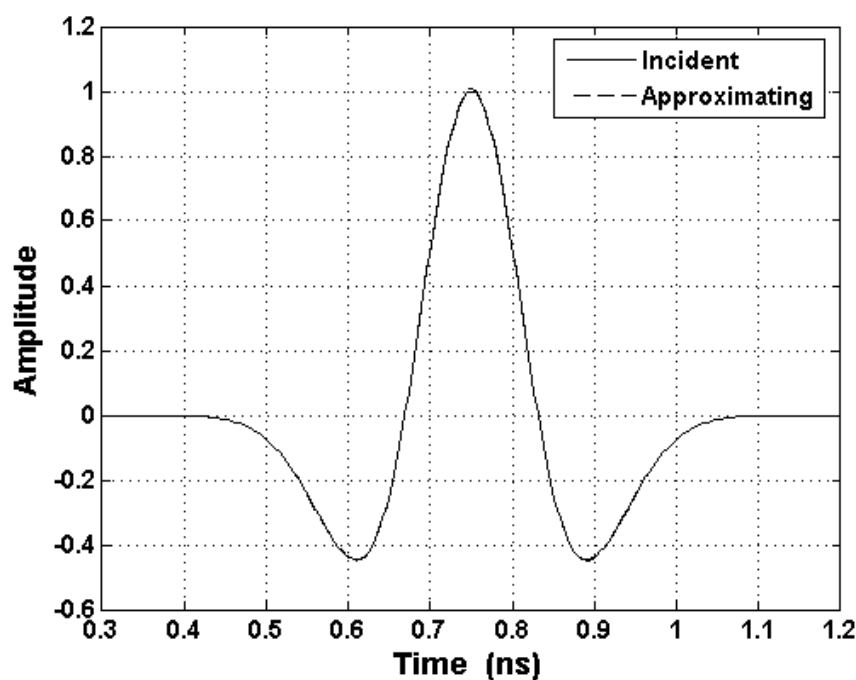

Fig. 1. Incident pulse and approximating pulse with 40 exponentials.
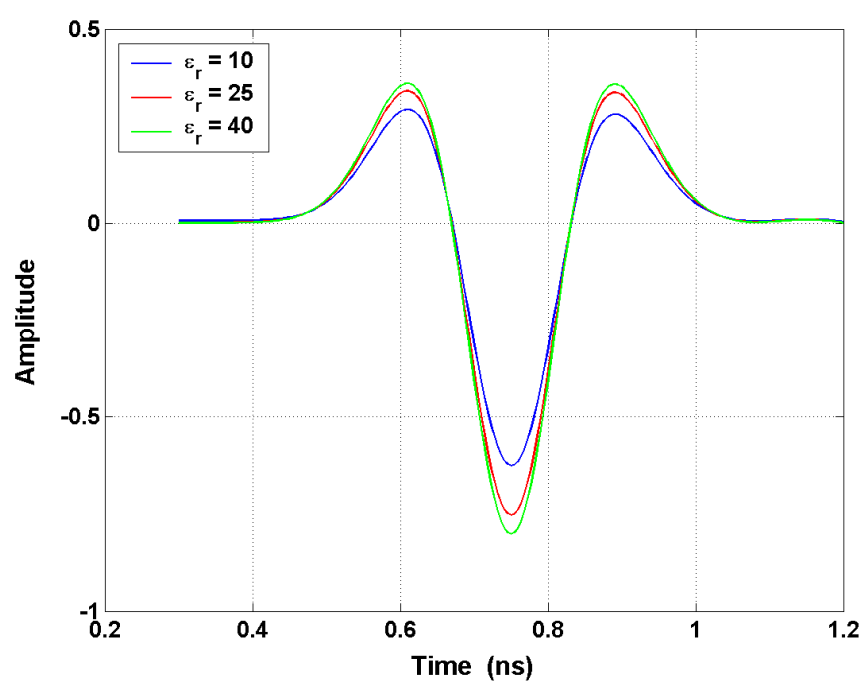
Fig. 2. Reflected field for the horizontal polarization ($\theta = 45^0$, $\varepsilon_r = 10, 25, 40$ and $\sigma = 0.1$ mho/m).
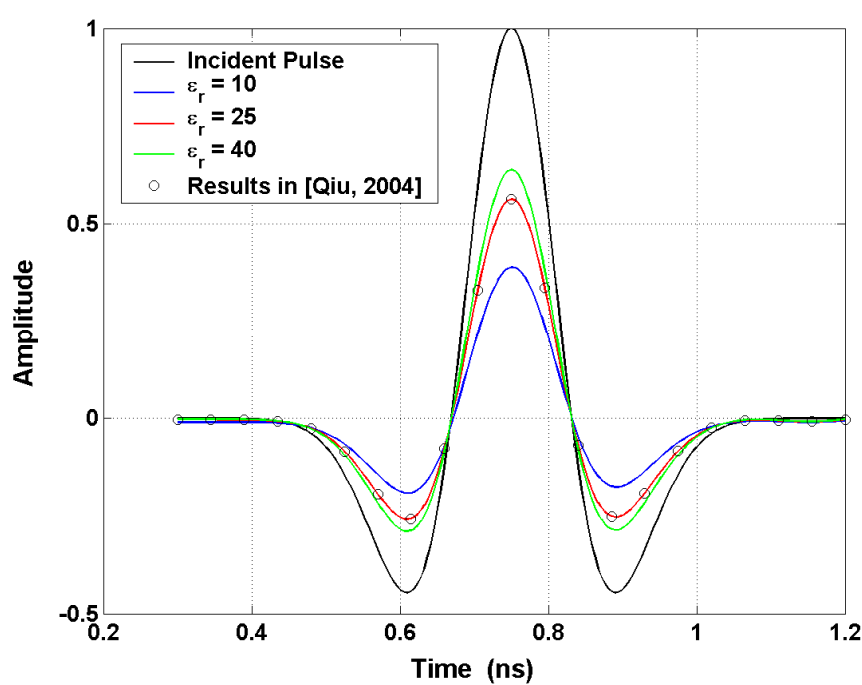

Fig. 3. Reflected field for the vertical polarization ($\theta = 45^0$, $\varepsilon_r = 10, 25, 40$ and $\sigma = 0.1$ mho/m).

5. Performance Analysis of UWB Communication in a Hallway Environment

Recently pulse distortion in time domain (or frequency dependence in frequency domain) has received considerable attention (Qiu, 2006). Studies on pulse distortion are important in various areas including channel modeling (Qiu, 2004) and UWB system analysis and design. So far, in the most investigations, the received UWB signal waveforms are assumed on the basis of measurement data for some kind of transmitted signals and specific scenarios (Ramírez-Mireles, 2002). This approach for determining received waveforms could not have generality. It would be difficult to use this approach to clarify the mechanisms causing pulse shape distortion and to connect system performance parameters such as bit error rate (BER) with propagation environment parameters such as transmitter and receiver heights, transmitter-receiver separations, wave polarizations, material parameters of reflecting surfaces, etc.

A new theoretical framework is being set up currently (Qiu, 2004) (Qiu, 2006), making it possible to predict UWB system performances directly from propagation environment parameters. In a multipath channel, normally reflected waves have most significant impacts on pulse distortion. In the new framework, the impulse response of a lossy interface developed in (Barnes & Tesche, 1991) is utilized, and then reflected waves are evaluated in time domain by convolving the incident field waveform with the impulse response. This impulse response contains an infinite sum of modified Bessel functions that evaluates the response term persisting in time. In order to apply this expression to practical problems, truncation of the infinite sum of modified Bessel functions is needed. Few terms permits a simple evaluation but makes the accuracy degrade, while many more terms are required to approach an acceptable accuracy but makes calculation complicated and time-consuming. Furthermore, this impulse response was derived from the approximate Fresnel reflection coefficient, which holds under the conditions that the relative dielectric constant ε_r is on the order of 10 or more and that the incident angle θ with the interface is small. Hence, the accuracy of the evaluation of reflected waves is questionable for incident angles larger than 80^0 and/or ε_r less than 10, particularly for vertical polarization.

In this section, a time domain multipath model is utilized to characterize UWB signal propagation in a hallway. Transient waves reflected from conducting interfaces for both vertical and horizontal incidence are calculated through numerical inversion of Laplace transform, which is simple and accurate. With the evaluation of direct and reflected waves in time domain, the performance analysis is conducted for binary UWB communications, and the impacts of multipath signals on pulse distortion and UWB system performance are discussed. This approach does not need the conditions on the relative dielectric constant ε_r and the incident angle θ, and can achieve satisfactory accuracy in both late and early time.

This work is classified as "deterministic channel modeling", and has a conceptual foundation based on per-path pulse shapes. The signal model is such that the received deterministic signals governed by electromagnetic wave equations are distorted by the background noise. The system model is such that the receiver is optimal in some sense, which is determined by the statistical communication theory. The wave-based solutions provide the response of the channel where each wave arrives separately. The availability of the channel response allows the receiver to match with the entire received signal composed of a linear superposition of

many mutipath pulses. Hence, the system performance is jointly determined by electromagnetic and statistical communication theories.

Hallway is a special indoor environment in the sense of its long and narrow geometrical configuration, where the light of sight (LOS) ray together with multiple reflection rays dominate the received signal. In a hallway whose size is quite large relative to wavelength of UWB signal, ray tracing should be applicable. Furthermore, because of the transient characteristics of UWB pulses, it should be more convenient to analyze the performance of UWB communication in time domain. Specular reflection is assumed for all the reflections undergoing in a hallway environment, which is resonable considering the roughness of the walls is far less than the wavelength of the propagation signal. It is also assumed that all the reflection interfaces are made of the same material (Zhou & Qiu, 2006).

Fig. 4 illustrates the direct (light of sight) path AB, single reflection paths AC_1B and AC_2B, double reflection paths AD_1E_2B and AD_2E_1B, triple reflection paths $AF_1G_2H_1B$ and $AF_2G_1H_2B$, fourfold reflection paths $AI_1J_2K_1L_2B$ and $AI_2J_1K_2L_1B$. In the following analysis, it is assumed that the multipath signals through the fivefold and multifold reflection paths have smaller magnitudes than the signals via the less than fivefold reflection paths. Then the signals through the direct, single, double, triple and fourfold reflection paths are only taken into account in the performance analysis of a binary UWB communication system. Furthermore, the reflected rays are divided into two groups: one is for those with the first reflection occuring on the floor (AC_1B, AD_1E_2B, $AF_1G_2H_1B$ and $AI_1J_2K_1L_2B$); another one is for those with the first reflection happening on the ceiling (AC_2B, AD_2E_1B, $AF_2G_1H_2B$ and $AI_2J_1K_2L_1B$).
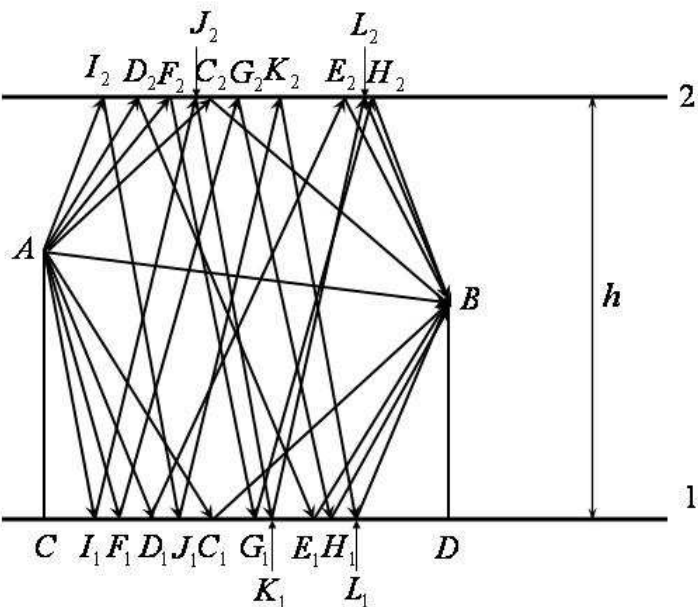

Fig. 4. UWB signal propagation in a hallway environment. AC=1.8 m, BD=1.5 m, $h = 3$ m, CD=2.0 m, $\varepsilon_r = 25$, $\sigma = 0.1$ S/m.

The electric field of a ray from the transmitter to the receiver can be calculated by the following equations.

For the direct ray,

$$E_{LOS}(s) = E(s)\frac{exp(-jkr_0)}{r_0} \tag{27}$$

where $E(s)$ is the electric field emitted by the transmitter in complex frequency (s) domain and can be accurately and approximately given by (14) for any exponential and non exponential signals, respectively, k is the wave number, r_0 is the distance that the ray travels from the transmitter to the receiver and is given by

$$r_0 = \sqrt{(h_t - h_r)^2 + d^2} \tag{28}$$

with d representing the distance of the transmitter-receiver separation (CD) and h_t and h_r representing the heights of transmitting and receiving antennas (AC and BD), respectively.

For reflected rays,

$$E_{reflected}(s) = [R(s)]^i E(s)\frac{exp(-jkr_i)}{r_i} \tag{29}$$

where $R(s)$ is reflection coefficient in s domain and is given by (12) and (13) for vertical and horizontal polarizations, respectively, and r_i is the length of the reflection path, along which the ith ray travels and undergoes i-fold reflections, and is given by

$$r_i = \sqrt{l_i^2 + d^2} \tag{30}$$

with

$$l_i = \begin{cases} (h_t + h_r) + (i-1)h & i\ is\ odd \\ (h_t - h_r) + ih & i\ is\ even \end{cases}, \tag{31}$$

where h is the height of the hallway. For different rays, reflection angles in $R(s)$ are different. The reflection angle for the ith ray, θ_i, can be determined by

$$\theta_i = arctan\left(\frac{d}{r_i}\right). \tag{32}$$

The contribution from the first group of reflected rays can be expressed as

$$E_{group1}(s) = \sum_{i=1}^{I} [R(s)]^i E(s)\frac{exp(-jkr_i)}{r_i} \tag{33}$$

with $I = 4$ corresponding to the case in Fig. 4 where the rays with a maximum of 4 reflections have been traced.

Since the second group of reflected rays follow the same laws as the first group of reflected rays, we can still use (33) and simply replace h_t and h_r with $h - h_t$ and $h - h_r$, respectively, to obtain the contribution from the second group of reflected rays, $E_{group2}(s)$.

The total received electric field at the receiver is given by

$$E_{total}(s) = E_{LOS}(s) + E_{group1}(s) + E_{group2}(s).$$ (34)

The corresponding waveform $E_{total}(t)$ can be achieved using numerical inversion of Laplace transform based on the discussion in Section 4. With a signal waveform $f(t)$, one of the most important system performance parameters, bit error rate (BER), can be determined by the equations below (Ramírez-Mireles, 2002).

The normalized signal correlation function of $f(t)$ is defined as the inner product of $f(t)$ with a shifted version $f(t-\tau)$

$$\gamma(\tau) = \frac{1}{E_f} \int_{-\infty}^{\infty} f(t) f(t-\tau) dt$$ (35)

where

$$E_f = \int_{-\infty}^{\infty} |f(t)|^2 dt$$ (36)

is the energy of the signal. Hence, if the received signal is $f(t)$, the squared distance between received signals is

$$d^2(\tau) = \frac{1}{2E_f} \int_{-\infty}^{\infty} |f(t) - f(t-\tau)|^2 dt = (1 - \gamma(\tau)).$$ (37)

The binary bit error rate (BER) is

$$P_e(\tau) = Q\left(\sqrt{\frac{\Lambda \cdot d^2(\tau)}{2}}\right)$$ (38)

where Λ is the signal-to-noise (SNR) value and $Q(\bullet)$ denotes the Gaussian tail integral.

We still use the normalized Gaussian doublet pulse, given by equation (26) but with the waveform parameter τ_p = 6 ns and the time shift t_s = 15 ns. Fig. 5 plots the direct field, reflected fields and total received field at the receiver for vertical and horizontal polarizations. Fig. 6 shows the bit error rates (BERs) of non-multipath (Gaussian) and multipath channels for vertical and horizontal polarizations, which are calculated on the basis of the waveforms in Fig. 5.

Fig. 5 and Fig. 6 demonstrate that the multipath components with one, two and three reflections have significant impacts on the waveforms of received signals and on the system performance. Fig. 6 shows no significant difference between the impacts of the components through triple and fourfold reflection paths, indicating that multipath components with five and more reflections can be ignored. Moreover, it can be seen from Fig. 6 that multipath signals have a larger influence on the bit error rate for vertical polarization than for horizontal polarization.
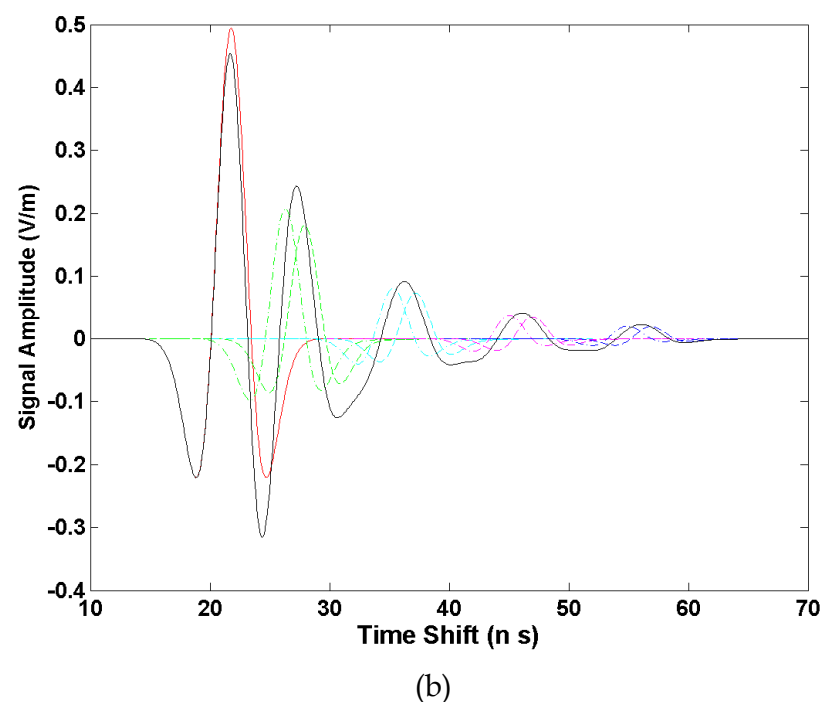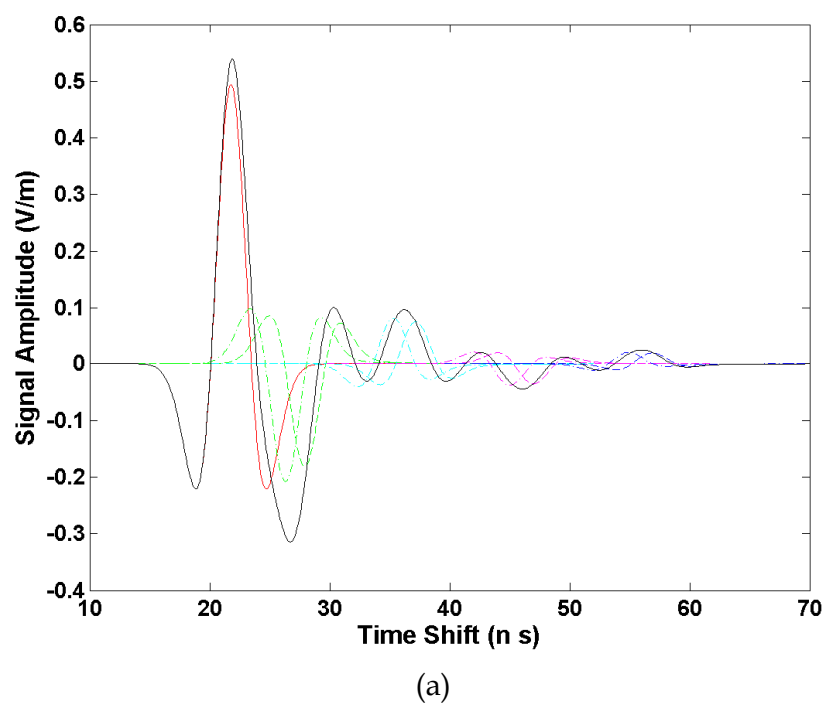
(a)

(b)

Fig. 5. Waveforms of direct field, reflected fields and their summations at receiver.
(a) horizontal polarization; (b) vertical polarization.
Red solid line: direct (LOS) path AB;
Green dashed and dash-dot lines: single reflection path AC_1B and AC_2B;
Cyan dashed and dash-dot lines: double reflection paths AD_1E_2B and AD_2E_1B;
Magenta dashed and dash-dot lines: triple reflection paths $AF_1G_2H_1B$ and $AF_2G_1H_2B$;
Blue dashed and dash-dot lines: fourfold reflection paths $AI_1J_2K_1L_2B$ and $AI_2J_1K_2L_1B$;
Black solid line: total received field.

(a)

(b)
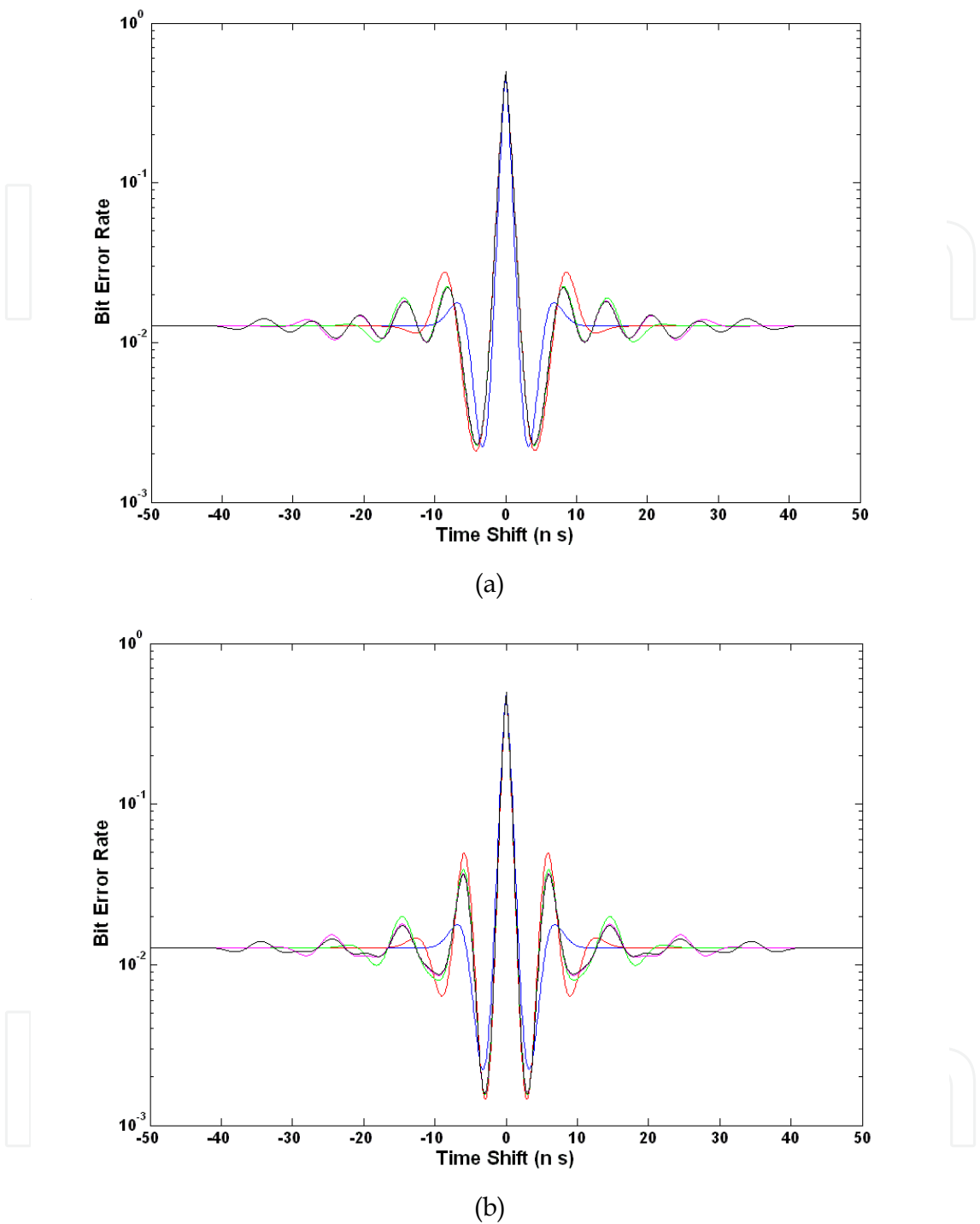
Fig. 6. Time-domain bit error rates of non-multipath channel AB (blue line), multipath channels $AB + AC_1B + AC_2B$ (red line), $AB + AC_1B + AC_2B + AD_1E_2B + AD_1E_2B$ (green line), $AB + AC_1B + AC_2B + AD_1E_2B + AD_1E_2B + AF_1G_2H_1B + AF_2G_1H_2B$ (magenta line), and $AB + AC_1B + AC_2B + AD_1E_2B + AD_1E_2B + AF_1G_2H_1B + AF_2G_1H_2B + AI_1J_2K_1L_2B + AI_2J_1K_2L_1B$ (black line) for (a) horizontal polarization and (b) vertical polarization.

6. Propagation of UWB Pulses through a Lossy Dielectric Slab

The transient analysis of pulses propagating through a lossy dielectric slab is of great significance in a number of engineering fields, such as material characterization and diagnosis, wall penetration radar, and pulse radio. In fact, this kind of analysis can provide valuable insights into the appreciation of the capabilities and limitations of UWB communication for indoor and indoor-outdoor scenarios. As discussed in Section 2, the approximation to a frequency-domain reflection coefficient permits one analytical expression of the impulse response of a lossy half space (Barnes & Tesche, 1991), but makes the solutions inaccurate or even invalid in some cases, e.g., for large incident angles. Based on the approximate form in (Barnes & Tesche, 1991), the time domain solutions for pulse transmission through a lossy dielectric slab were achieved and some related UWB issues were addressed (Qiu, 2004) (Chen et al., 2004). These solutions contain infinite sums of modified Bessel functions and time domain convolutions, and are implemented in three directions, parallel polarization, normal and tangential perpendicular polarizations (Chen et al., 2004), leading to considerable calculations.

In this section, based on the discussion in Section 3 and Section 4, the technique combining numerical inversion of Laplace transform with Prony's method is extended to the transient analysis of pulses propagating through a lossy dielectric slab. Comparison between our results obtained and those obtained using the FDTD technique indicates a good agreement. The waveforms and strengths of the transmitted signals are governed by four main parameters, thickness, relative permittivity and conductivity of the slab and incident angles. The analysis of transmitted signal waveforms is conducted for four different parameters and the results are shown to be comparable to those given by (Chen et al., 2004). Based on this waveform analysis, the transmission loss is discussed for different parameters and the results are shown to be consistent with the previously published results (Chen et al., 2004). Our approach also yields the results for a large incident angle, these being unavailable using alternative approaches (Chen et al., 2004).
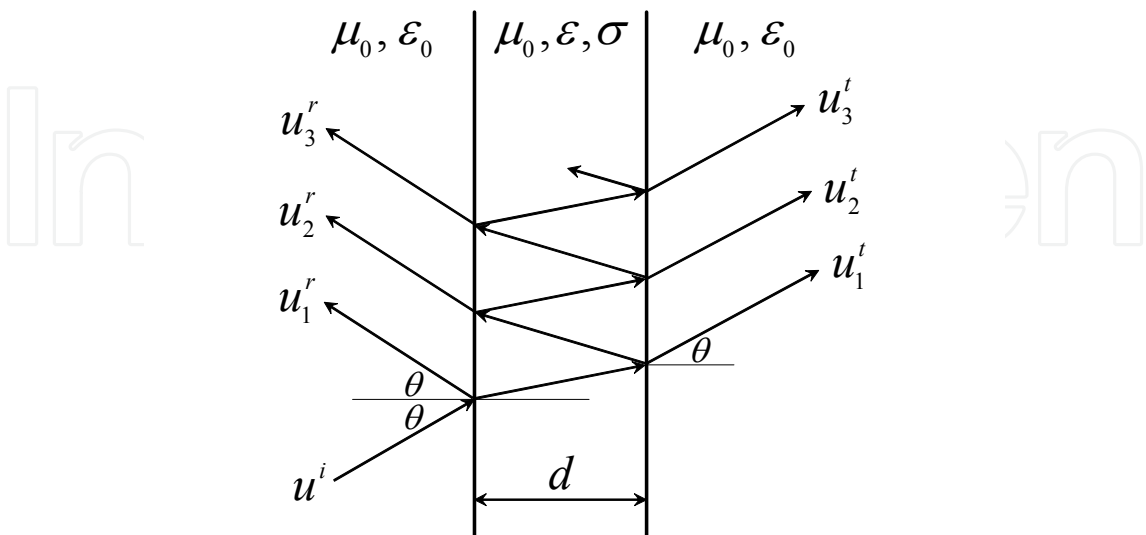

Fig. 7. Pulse is impinging on lossy dielectric slab.

In this investigation, the Gaussian doublet pulse with the same waveform parameter and time shift as in Section 4 is used as the incident pulse. Fig. 7 shows that the pulse is impinging on a homogeneous lossy slab at an incident angle of θ. The slab has an thickness of d, permeability of μ_0, conductivity σ and permittivity of $\varepsilon = \varepsilon_0 \varepsilon_r$ where ε_0 is the permittivity of vacuum and ε_r is the relative permittivity of the slab. The transmission through a dielectric layer is governed by the equation (Yeh, 1988)

$$T = \frac{t_{0n} \, t_{n0} \, e^{-j\varphi}}{1 - r_{0n} \, r_{n0} \, e^{-j2\varphi}} \tag{39}$$

where r and t denote the reflection and transmission coefficients of the interface, respectively. The subscripts $0n$ and $n0$ mean that the pulse is incident from air onto the layer and from the layer onto air. The quantity φ is the complex frequency dependent electrical length of the layer as seen by the wave and is given by

$$\varphi(s) = \frac{s}{j} \frac{d}{c} \sqrt{\varepsilon_r - \sin^2 \theta + \frac{\sigma}{s \varepsilon_0}} \tag{40}$$

s is the complex frequency and c is the phase velocity of the wave in vacuum. With $t_{0n} t_{n0} - r_{0n} r_{n0} = 1$ and $r_{0n} = -r_{n0}$ (Yeh, 1988), (39) is written as

$$T(s) = \frac{\left(1 - r_{0n}^{\,2}(s)\right) e^{-j\varphi(s)}}{1 - r_{0n}^{\,2}(s) \, e^{-j2\varphi(s)}} \tag{41}$$

where $r_{0n}(s)$ is the reflection coefficient in complex frequency domain and is given by (12) for vertical polarization, or by (13) for horizontal polarization.

The image function of the approximating pulse is

$$E^{inc}(s) = \sum_{p=1}^{q} \frac{C_p}{s + \alpha_p}. \tag{42}$$

The final image functions is

$$F(s) = T(s) E^{inc}(s). \tag{43}$$

It satisfies the four conditions specified in Section 3 under which $f(t)$ can be approximated by $f_{ec}(t, \rho)$. For $s = [\rho + j(n - 0.5)\pi]/t$, $F(s)$ does not obey the two additional conditions in Section 3 under which $f_{ec}^{lm}(t, \rho)$ can be used to approximate $f_{ec}(t, \rho)$.

The total transmitted field can be decomposed into a series of successive transmitted components,

$$T = u_1^t + u_2^t + u_3^t + \cdots = t_{0n} t_{n0} e^{-j\varphi} \left[1 + r_{n0}^{\ 2} e^{-j2\varphi} + \left(r_{n0}^{\ 2} e^{-j2\varphi} \right)^2 + \cdots \right]. \tag{44}$$

Consider the first term modeling two transmissions through two surfaces of the layer,

$$u_1^t = t_{0n} t_{n0} e^{-j\varphi} = \left(1 - r_{0n}^{\ 2} \right) e^{-j\varphi}. \tag{45}$$

$F_1(s) = u_1^t(s) E^{inc}(s)$ still does not satisfy the two additional conditions for Euler summation due to the phase factor $e^{-j\varphi}$ when $s = [\rho + j(n - 0.5)\pi]/t$.

From (40), it is observed that, when $s \to \infty$,

$$\varphi(s) \to \varphi_m(s) = \frac{s}{j} \frac{d}{c} \sqrt{\varepsilon_r - \sin^2\theta}. \tag{46}$$

The replacement image function for $F_1(s)$ is defined as

$$F_{r1}(s) = u_1^t(s) E^{inc}(s) e^{j\phi_m(s)} = F_1(s) e^{s\tau} \tag{47}$$

and satisfies the four conditions and the two additional conditions listed in Section 3, where $e^{j\varphi_m(s)}$ is the modifying phase factor and the time shift is

$$\tau = \frac{d}{c} \sqrt{\varepsilon_r - \sin^2\theta}. \tag{48}$$

Hence, (7) is applicable to calculate $f_{r1,ec}^{lm}(t,\rho)$ which approximates $f_{r1,ec}(t,\rho)$, the original function of $F_{r1}(s)$. From (47), the relationship between $f_{r1,ec}^{lm}(t,\rho)$ and $f_{1,ec}^{lm}(t,\rho)$ which approximates $f_{1,ec}(t,\rho)$, the original function of $F_1(s)$, is given by

$$f_{1,ec}^{lm}(t,\rho) = f_{r1,ec}^{lm}(t - \tau, \rho). \tag{49}$$

Similarly, consider the second term in (44), which characterizes two transmissions through two surfaces and two reflections between two surfaces,

$$u_2^t = t_{0n} t_{n0} r_{n0}^2 e^{-j3\varphi} = \left(1 - r_{0n}^{\ 2} \right) r_{n0}^2 e^{-j3\varphi}. \tag{50}$$

$F_2(s) = u_2^t(s) E^{inc}(s)$ does not satisfy the two additional conditions specified in Section 3 due to the phase factor $e^{-j3\varphi}$ when $s = [\rho + j(n - 0.5)\pi]/t$. The replacement image function for $F_2(s)$ is

$$F_{r2}(s) = u_2^t(s) E^{inc}(s) e^{j3\phi_m(s)} = F_2(s) e^{3s\tau} \tag{51}$$

and meets the four conditions in Section 3 and the two additional conditions for Euler summation. $f_{r2,ec}^{lm}(t,\rho)$ can be calculated by using (7), and is a good approximation to $f_{r2,ec}(t,\rho)$, the original function of $F_{r2}(s)$. From (51), the relationship between $f_{r2,ec}^{lm}(t,\rho)$ and $f_{2,ec}^{lm}(t,\rho)$ which approximates $f_{2,ec}(t,\rho)$, the original function of $F_2(s)$, is given by

$$f_{2,ec}^{lm}(t,\rho) = f_{r2,ec}^{lm}(t - 3\tau, \rho). \tag{52}$$

Following the above procedure, $f_{i,ec}^{lm}(t,\rho)$ can be achieved and is a good approximation to $f_{i,ec}(t,\rho)$, the original functions of $F_i(s) = u_i^t(s) E^{inc}(s)$, $i = 1, 2, 3, \cdots$. From

$$F = F_1 + F_2 + F_3 + \cdots, \tag{53}$$

the final original function can be given approximately by

$$\begin{aligned} f(t) \approx f_{ec}(t,\rho) &= f_{1,ec}(t,\rho) + f_{2,ec}(t,\rho) + f_{3,ec}(t,\rho) + \cdots \\ &\approx f_{1,ec}^{lm}(t,\rho) + f_{2,ec}^{lm}(t,\rho) + f_{3,ec}^{lm}(t,\rho) + \cdots \end{aligned} \tag{54}$$

In general, the terms beyond the first term have much weaker impacts than the first one in (54), and then only taking the first term $f_{r1,ec}^{lm}(t,\rho)$ leads to a high accuracy. If a very high accuracy is required for some specific purposes, the first several terms in (54) will be added together. In the following discussion, only the first term in (54) is taken into account. Fig. 8 plots the waveform of the transmitted pulse at the layer's back surface, and shows that our results agree quite well with FDTD results. The comparison between our results and FDTD results for vertical polarization also leads to a quite good agreement but is omitted here to save the space.

Figures 9-12 illustrate the waveforms of the transmitted signal through a slab with different thickness, relative permittivity, conductivity and incident angles. With reference to the incident pulse shown in Fig. 1, the attenuation, delay and distortion of the transmitted pulse can be seen and compared with each other in the different cases. Fig. 9 shows that the amplitude of the transmitted signal decreases, the delay increases and the distortion becomes larger with the increase of the thickness. In Fig. 10, the amplitude becomes a little smaller, the distortion becomes a little larger and it takes longer for the pulse to go through the layer as the relative permittivity increases. Fig. 11 illustrates that the amplitude decreases, the distortion increases but the delay almost remain the same when the conductivity increases.
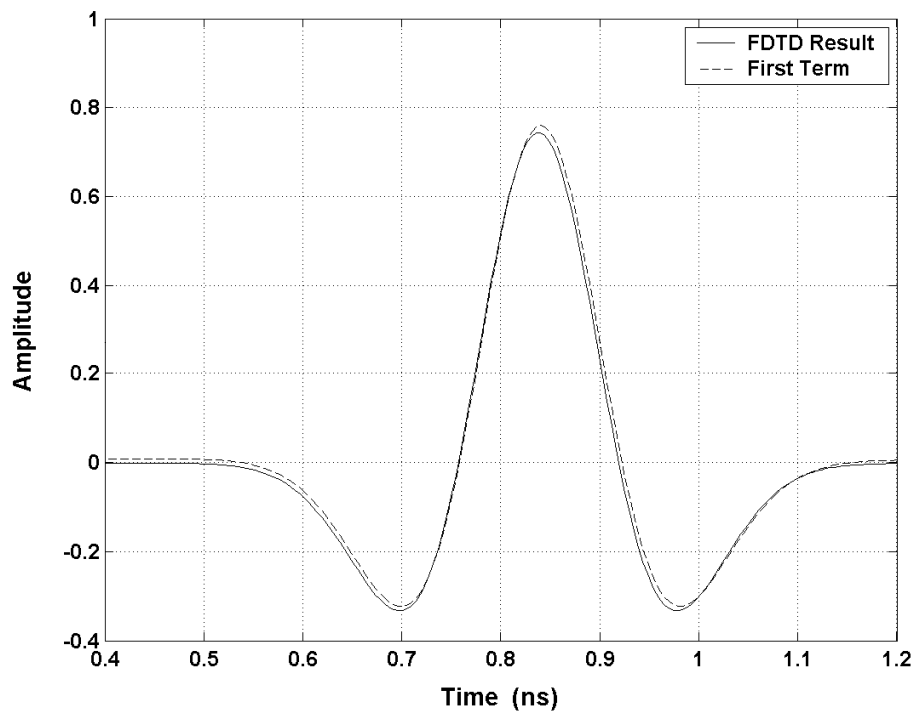
Fig. 8. Waveforms of transmitted signal obtained using this method and using FDTD for horizontal polarization. $d = 0.02$ m, $\varepsilon_r = 2$, $\sigma = 0.1$ S/m and $\theta = 30^0$.
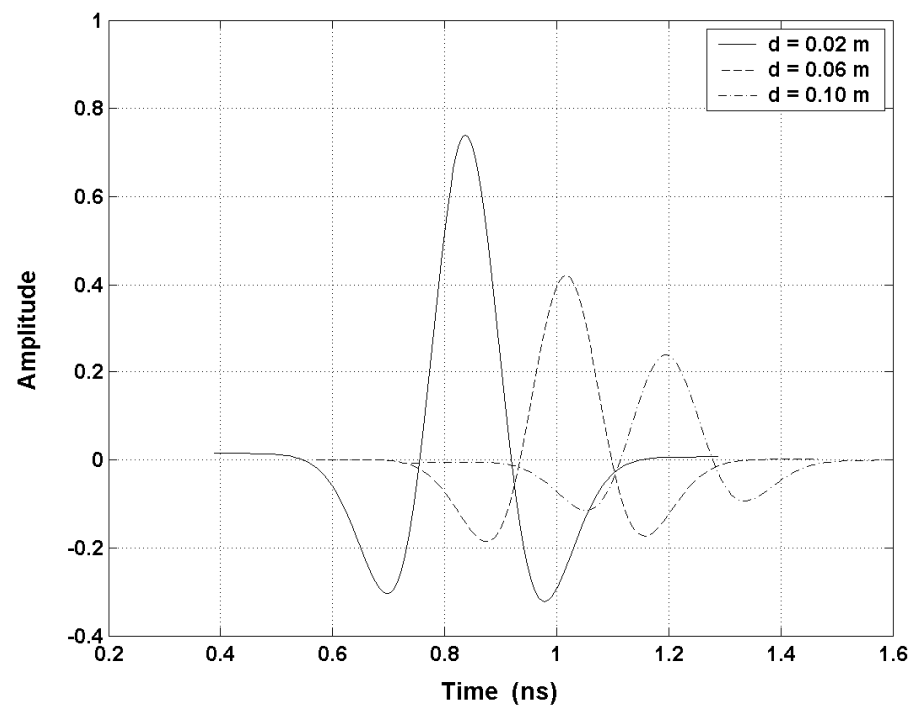

Fig. 9. Waveforms of transmitted signal for horizontal polarization. Varying d, $\varepsilon_r = 2$, $\sigma = 0.1$ S/m and $\theta = 30^0$.
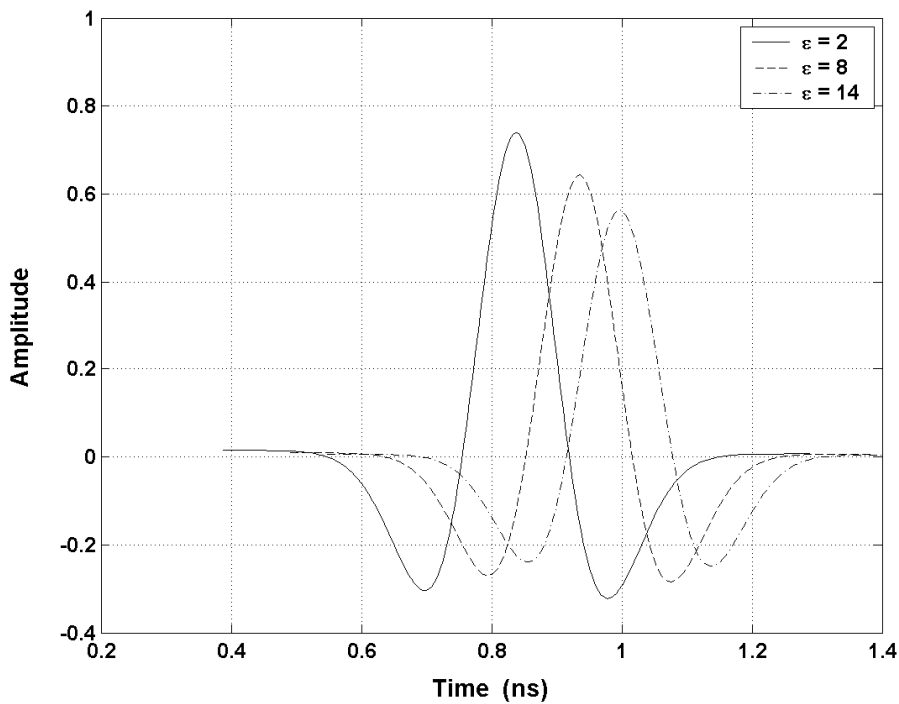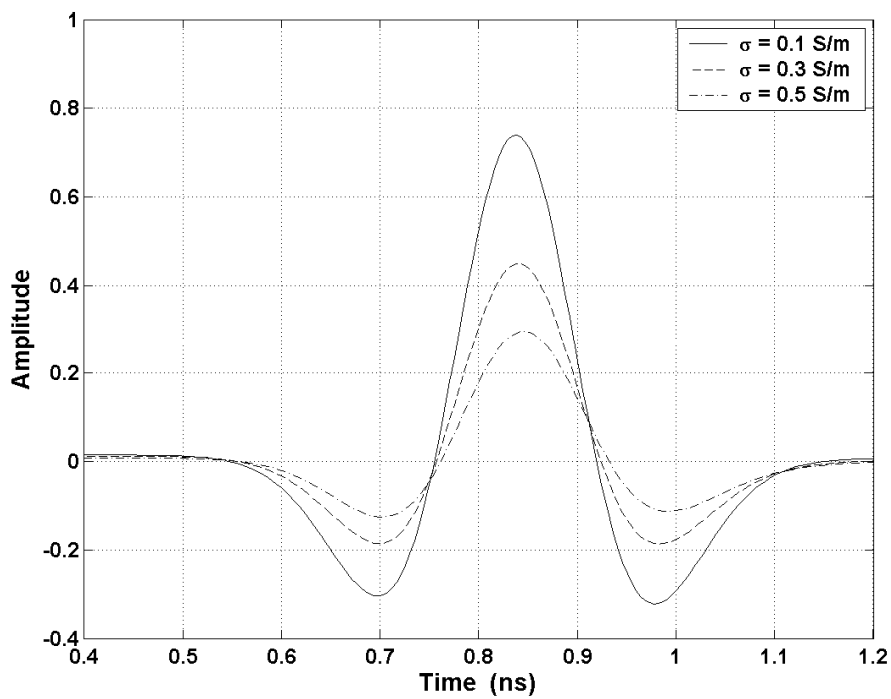
Fig. 10. Waveforms of transmitted signal for horizontal polarization. Varying ε_r, $d = 0.02$ m, $\sigma = 0.1$ S/m and $\theta = 30^0$.

Fig. 11. Waveforms of transmitted signal for horizontal polarization. Varying σ, $d = 0.02$ m, $\varepsilon_r = 2$ and $\theta = 30^0$.
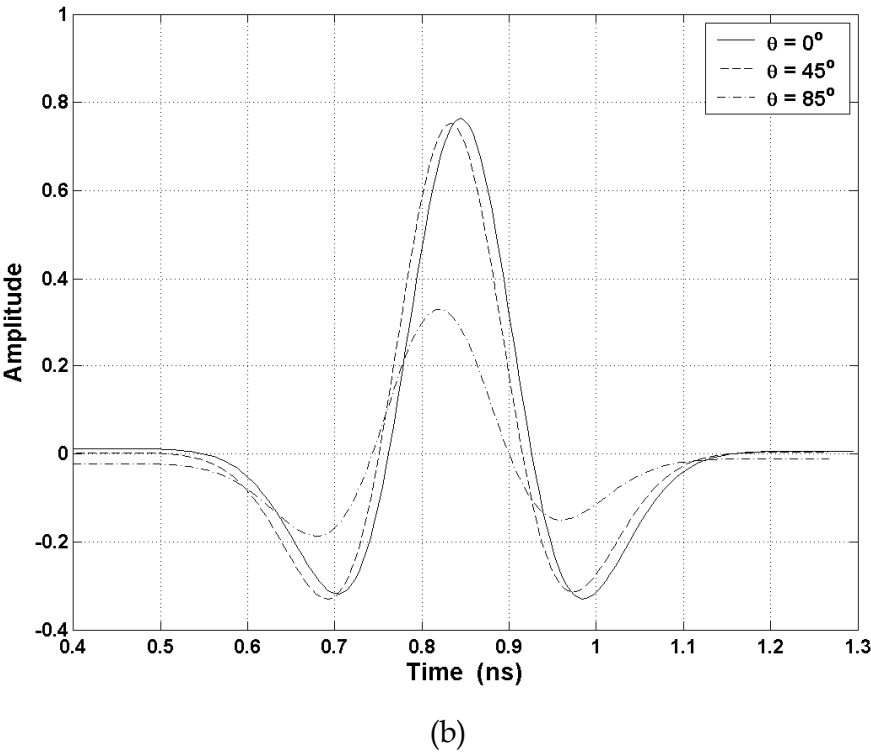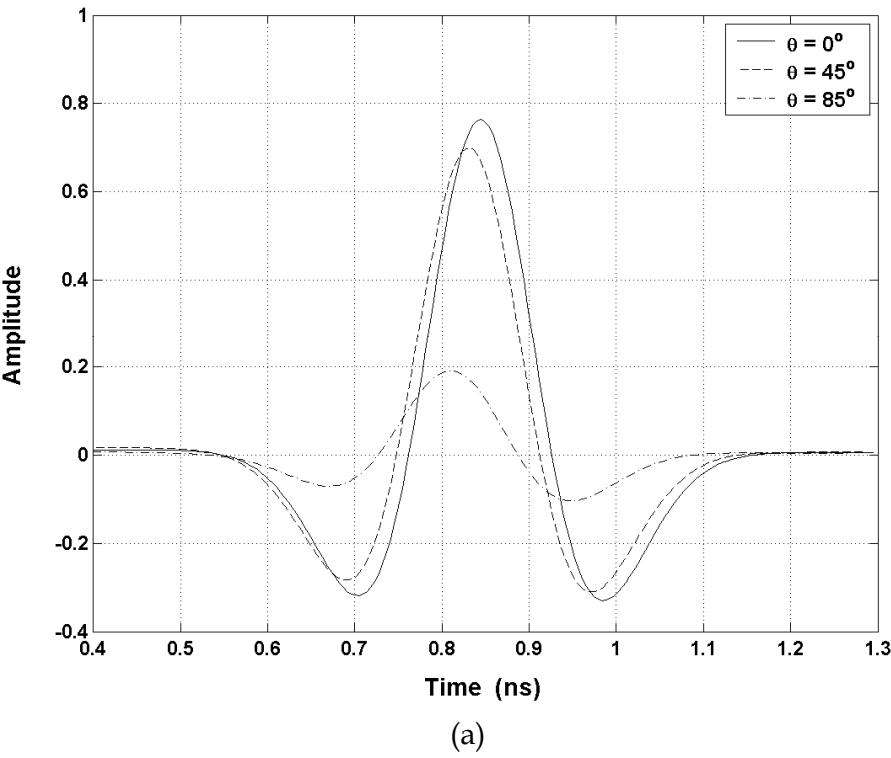
(a)

(b)

Fig. 12. Waveforms of transmitted signal. (a) horizontal polarization; (b) vertical polarization. Varying θ, $d = 0.02$ m, $\varepsilon_r = 2$ and $\sigma = 0.1$ S/m.

Although Figures 9-11 plot the results only for horizontal polarization due to a limited space, it is worthwhile to indicate that, when the incident angle is fixed and the other three parameters are varying, the transmitted pulse experiences roughly the same variation for both polarizations in the above three cases. On the other hand, when the incident angle is varying, the transmitted pulse undergoes different variations for two different polarizations. As shown in Fig. 12, when the incident angle increases, the amplitude decreases, the delay decreases slightly and the distortion becomes larger. Meanwhile, the transmitted pulse undergoes larger variation for horizontal polarization than for vertical polarization. The above results accord with those in (Chen et al., 2004). Nevertheless, Fig. 12 demonstrates that the amplitude and distortion largely change when the incident angle is close to 90^0. This case was not discussed in (Chen et al., 2004).

On the basis of the above results, the transmission loss through a layer is discussed for different parameters. Fig. 13 (a) illustrates that the transmission loss is basically proportional to the thickness and increases with the increase of the conductivity. As the conductivity becomes larger, the change rate of the transmission loss with the thickness becomes larger. Fig. 13 (b) shows that the transmission loss has the minimal value for a normal incidence, and slightly increases as the relative permittivity increases. The comparison between Fig. 13 (a) and Fig. 13 (b) indicates that the thickness and conductivity have much larger impacts on the transmission loss than the other two parameters, the relative permittivity and incident angle. These conclusions are consistent with those drawn in (Chen et al., 2004). In Fig. 13 (b), it is seen that the transmission loss for the incident angle close to 90^0 is much larger, and increases much faster with the increase of the relative permittivity than that for a small incident angle, which is not addressed in (Chen et al., 2004) and then is added here.

7. Additional Comments

As is well known, the principle of causality stating that the response cannot come before the stimulus leads to the Kramers–Kronig relations describing the interdependence of the real and imaginary parts of the susceptibility $\chi(\omega)$ (Rothwell & Cloud, 2001). The Kramers–Kronig relations compose one of the most elegant and general theorems in physics, since they depend for their validity only on the principle of causality. As applied to wave propagation, the real part of susceptibility describes essentially the index of refraction and imaginary part the absorbstion coefficient of a medium. Thus, the Kramers–Kronig relations explain in the most fundamental and general terms, completely independent of the underlying physical mechanisms, the intimate connection between refraction and absorption. Actually, given one, the other follows immediately. The Kramers–Kronig relations are given by

$$\mathrm{Re}\big[\chi(\omega)\big]=\frac{1}{\pi}P\int_{-\infty}^{\infty}\frac{\mathrm{Im}\big[\chi(\Omega)\big]}{\omega-\Omega}\,d\Omega \tag{55}$$

$$\mathrm{Im}\big[\chi(\omega)\big]=-\frac{1}{\pi}P\int_{-\infty}^{\infty}\frac{\mathrm{Re}\big[\chi(\Omega)\big]}{\omega-\Omega}\,d\Omega \tag{56}$$

where P stands for principal part. The expressions show that causality requires the real and imaginary parts of the dielectric susceptibility (permittivity) or magnetic susceptibility (permeability) to depend on each other through the Hilbert transform pair.
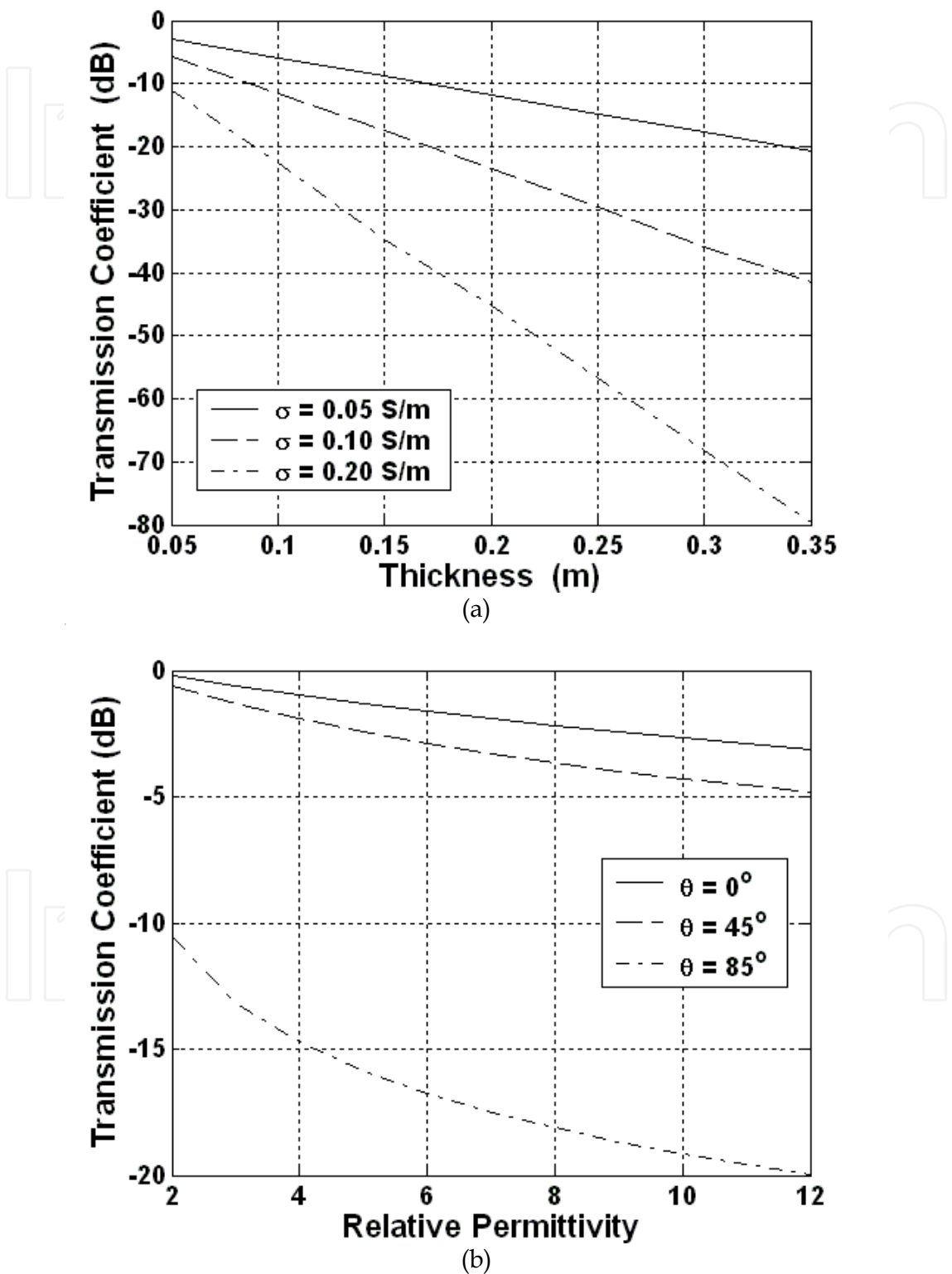

(a)

(b)

Fig. 13. Transmission coefficient of slabs with different parameters. (a) thickness and conductivity; (b) relative permittivity and incident angle.

In Section 4 and Section 6, $\varepsilon(\omega)$ varies when $\sigma(\omega)$ is fixed, and $\sigma(\omega)$ varies when $\varepsilon(\omega)$ is fixed. This seems not to obey the Kramers–Kronig relations but can be considered as the approximations of permittivity and conductivity of a conductive dielectric at low frequencies. The complex permittivity of a dielectric is best described by the resonance model (Rothwell & Cloud, 2001)

$$\varepsilon_c(\omega) = \varepsilon(\omega) + j\,\varepsilon''(\omega) = \varepsilon(\omega) - j\,\frac{\sigma(\omega)}{\omega} = \varepsilon_0 + \sum_i \frac{\varepsilon_0\,\omega_{pi}^2}{\omega_i^2 - \omega^2 + j\,\omega\,2\,\Gamma_i^2}, \tag{57}$$

where $\omega_{pi}^2 = N_i e^2 / m_i \varepsilon_0$ is the plasma frequency of the ith resonance component, and ω_i and Γ_i are the oscillation frequency and damping coefficient, respectively, of this component. Splitting the permittvity into real and imaginary parts we have

$$\varepsilon(\omega) = \varepsilon_0 \left(1 + \sum_i \frac{\omega_{pi}^2 \left(\omega_i^2 - \omega^2 \right)}{\left(\omega_i^2 - \omega^2 \right)^2 + 4\,\omega^2\,\Gamma_i^2} \right), \tag{58}$$

$$\varepsilon''(\omega) = -\varepsilon_0 \sum_i \frac{2\,\omega\,\Gamma_i\,\omega_{pi}^2}{\left(\omega_i^2 - \omega^2 \right)^2 + 4\,\omega^2\,\Gamma_i^2}, \tag{59}$$

and then

$$\sigma(\omega) = -\omega\,\varepsilon''(\omega) = \varepsilon_0 \sum_i \frac{2\,\omega^2\,\Gamma_i\,\omega_{pi}^2}{\left(\omega_i^2 - \omega^2 \right)^2 + 4\,\omega^2\,\Gamma_i^2}. \tag{60}$$

For low frequencies,

$$\varepsilon(\omega) \approx \varepsilon_0 \left(1 + \sum_i \frac{\omega_{pi}^2}{\omega_i^2} \right), \tag{61}$$

which is the static permittivity of material. A conductive dielectric has such small values of ω_i that the electrons become unbound. At low frequencies,

$$\sigma(\omega) \approx \varepsilon_0 \sum_i \frac{\omega_{pi}^2}{2\,\Gamma_i}, \tag{62}$$

which is the dc conductivity. Hence, it is not unreasonable for a conductive dielectric at low frequencies that $\varepsilon(\omega)$ and $\sigma(\omega)$ are approximately frequency independent and one of them varies when another is fixed. Even for modeling propagation of UWB signals in a typical band from 3 GHz to 10 GHz, the permittivity and conductivity of a construction material are still considered as constants independent in (Ghavami et al, 2004). In (Ho & Lai, 2007), the permittivity (or conductivity) of a lossy dielectric varies when the conductivity (or permittivity) is fixed. In (Suk, 2000), one of the permittivity, permeability and conductivity of a conductive medium varies when fixing the rest.

8. Conclusion

Numerical inversion of Laplace transform and Prony's method are discussed. The conditions under which numerical inversion of Laplace transform can be applied in practice are clarified. The approach combining numerical inversion of Laplace transform with Prony's method is applied to the analysis of transient reflection of UWB pulses from a conductive interface. Numerical results are illustrated and compared with those published in the literature. A good agreement between them validates the correctness and effectiveness of this approach.

With the evaluation of transient direct and reflected waves, the impacts of multipath components on pulse distortion and UWB system performance in a hallway environment are discussed. The significance of this work is twofold: First, the methodology combines the time domain electromagnetics and the UWB system theory, and lends us the powerful methods and rich solutions already available to gain insight into UWB problems. Second, the efficiency of the methodology is improved, leading to simple implementation, low computation cost, easy estimation and control of errors.

Based on the studies of pulses reflected from a conducting interface, characterization of pulses propagating through a lossy dielectric slab is pursued. Our results are shown to be comparable to the previously published results and agree well with those obtained using the FDTD technique. Furthermore, the corresponding results for an incident angle close to 90^0 can be provided with this technique, which can not be generated with the previous approaches. This efficient time domain technique can be extended in a straightforward manner to the transient analysis of multiple reflections and transmissions in lossy media, and thus provide a powerful tool for electromagnetic analysis and design.

9. References

Balanis, C. (1989). *Advanced Engineering Electromagnetics,* John Wiley & Sons, New York, NY, USA.

Barnes, P. & Tesche, F. (1991). On the direct calculation of a transient plane wave reflected from a finitely conducting half space. *IEEE Trans. Electromagn. Compat.,* Vol. 33, May 1991, pp. 90-96.

Chen, Z.; Yao, R. & Guo, Z. (2004) The characteristics of UWB signal transmitting through lossy dielectric slab. *Proceedings of IEEE Radio and Wireles Conference 2004*, pp. 134-138, Atlanta, GA, USA, Sept. 19–22, 2004.

Dudley, D.; Papazoglou, T. & White, R. (1974). On the interaction of a transient electromagnetic plane wave and a lossy half-space. *J. Appl. Phys.,* Vol. 45, Mar. 1974, pp. 1171-1175.

Ghavami, M.; Michael, L. & Kohno, R. (2004). *Ultra Wideband Signal and Systems in Communcation Engineering,* Section 4.3, pp. 110-121, John Wiley & Sons, Chichester, England; Hoboken, NJ, USA.

Ho, M. & Lai, F.-S. (2007). Effects of medium conductivity on electromagnetic pulse propagation onto dielectric half space: One-dimensional simulation using characteristic-based method. *J. Electromagn. Wave Appl.,* Vol. 21, No. 13, 2007, pp. 1773-1785.

Hosono, T. (1981). Numerical inversion of Laplace transform and some applications to wave optics. *Radio Sci.,* Vol. 16, No. 6, Nov.–Dec. 1981, pp. 1015–1019.

Klaasen, J. (1990). Time-domain analysis of one-dimensional electromagnetic scattering by lossy media. *Rep. FEL-90-A211,* TNO Phys. Electron. Lab., The Hague, Oct. 1990.

Maloney, J.; Smith, G. & Scott, Jr., W. (1990). Accurate computation of the radiation from simple antennas using the finite-difference time-domain method. *IEEE Trans. Antennas Propagat.,* Vol. 38, July 1990, pp. 1059-1068.

Maloney, J. & Smith, G. (1992). The use of surface impedance concepts in the finite-difference time-domain method. *IEEE Trans. Antennas Propagat.,* Vol. 40, Jan. 1992, pp. 38-48.

Pantoja, M.; Yarovoy, A. & Bretones, A. (2009). On the direct computation of the time-domain plane-wave refelction coefficients. *ACES (Applied Computational Electromgnetics Society) Journal,* Vol. 24, No. 3, June 2009, pp. 294-299.

Pao, H.-Y.; Dvorak, S. & Dudley, D. (1996, a). An accuate and efficient analysis for transient plane waves obliquely incident on a conductive half space (TE case). *IEEE Trans. Antennas Propagat.,* Vol. 44, No. 7, July 1996, pp. 918–924.

Pao, H.-Y.; Dvorak, S. & Dudley, D. (1996, b). An accuate and efficient analysis for transient plane waves obliquely incident on a conductive half space (TM case). *IEEE Trans. Antennas Propagat.,* Vol. 44, No. 7, July 1996, pp. 925–932.

Papazoglou, T. (1975). Transmission of a transient electromagnetic plane wave into a lossy half-space. *J. Appl. Phys.,* Vol. 46, Aug. 1975, pp. 3333-3341.

Qiu, R. (2004). A generalized time domain multipath channel and its application in ultra-wideband (UWB) wireless optimum receiver design–Part II: Physics-based system analysis. *IEEE Trans. Wireless Comm.,* Vol. 3, No. 6, Nov. 2004, pp. 2312–2324.

Qiu, R. (2006). A generalized time domain multipath channel and its application in ultra-wideband (UWB) wireless optimum receiver–Part III: System performance analysis. *IEEE Trans. Wireless Comm.,* Vol. 5, No. 10, Oct. 2006, pp. 2685–2695.

Ramírez-Mireles, F. (2002). Signal design for ultra-wide-band communications in dense multipath. *IEEE Trans. Veh. Tech.,* Vol. 51, No. 6, Nov. 2002, pp. 1517-1521.

Rothwell, E. & Cloud, M. (2001). *Electromagnetics,* Chapter 4, pp. 189-348, CRC Press, Boca Raton, FL, USA.

Rothwell, E. & Suk, J. (2003). Efficient computation of the time-domain TE plane-wave reflection coefficient. *IEEE Trans. Antennas Propagat.,* Vol. 51, No. 12, Dec. 2003, pp. 3283–3285.

Rothwell, E. (2005). Efficient computation of the time-domain TM plane-wave reflection coefficient. *IEEE Trans. Antennas Propagat.,* Vol. 53, No. 10, Oct. 2005, pp. 3417–3419.

Sommerfeld, A. (1914). Über die Fortpflanzung des Lichtes in dispergierenden Medien. *Ann. Phys.,* Vol. 44, 1914, pp. 177-202.

Stratton, J. (1941). *Electromagnetic Theory,* McGraw-Hill, New York, NY, USA.

Suk, J. (2000). *Transient analysis of plane-wave scattering in a layered medium,* Ph.D. dissertation, Michigna State University, East Lansing, MI, USA, December 2000.

Yeh, P. (1988). *Optical Waves in Layered Media,* pp. 66 and pp. 86–88, John Wiley & Sons, New York, NY, USA.

Zeng, Q. (2010). *Transient Analysis of Electromagnetic Waves Based on Numerical Inversion of Laplace Transform,* Ph.D. dissertation, University of Ottawa, Ottawa, Ontario, Canada, May 2010.

Zhou, C. & Qiu, R. (2006). Spatial focusing of time-reversed UWB electromagnetic waves in a hallway environment. *Proceedings of IEEE 38th Southeastern Symposium on System Theory,* Cookeville, TN, USA, 2006.
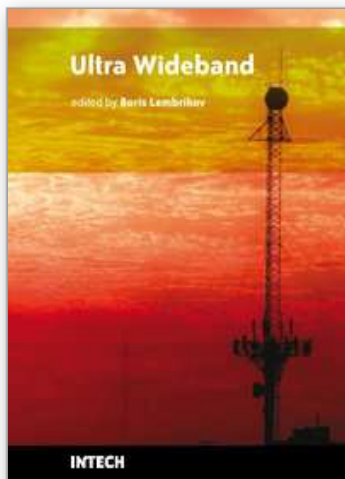
Ultra Wideband

Edited by Boris Lembrikov

Ultra wideband technology is one of the most promising directions in the rapidly developing modern communications. Ultra wideband communication system applications include radars, wireless personal area networks, sensor networks, imaging systems and high precision positioning systems. Ultra wideband transmission is characterized by high data rate, availability of low-cost transceivers, low transmit power and low interference. The proposed book consisting of 19 chapters presents both the state-of-the-art and the latest achievements in ultra wideband communication system performance, design and components. The book is addressed to engineers and researchers who are interested in the wide range of topics related to ultra wideband communications.

How to reference

In order to correctly reference this scholarly work, feel free to copy and paste the following:

Qingsheng Zeng and Arto Chubukjian (2010). Transient Modeling of Ultra Wideband Pulse Propagation, Ultra Wideband, Boris Lembrikov (Ed.), ISBN: 978-953-307-139-8, InTech, Available from: http://www.intechopen.com/books/ultra-wideband/transient-modeling-of-ultra-wideband-pulse-propagation

INTECH
open science | open minds